



RESEARCH ARTICLE

10.1002/2015GC006023

High-resolution paleomagnetic and sedimentological investigations on the Tibetan Plateau for the past 16 ka cal B.P.—The Tangra Yumco record

Key Points:

- PSV recorded in a lake from the Tibetan Plateau for the past 16 ka cal B.P.
- Inclination comparable to model predictions, East Asia PSV stack, and Lake Baikal
- Large-scale (<3000 km) geomagnetic field changes dominate this region

Karoline Henkel¹, Torsten Haberzettl¹, Guillaume St-Onge², Junbo Wang³, Marieke Ahlborn¹, Gerhard Daut¹, Liping Zhu³, and Roland Mäusbacher¹

¹Institute of Geography, Physical Geography, Friedrich Schiller University Jena, Jena, Germany, ²Institut des sciences de la mer de Rimouski, Université du Québec à Rimouski, Rimouski, Québec, Canada and GEOTOP Research Center, Canada,

³Institute of Tibetan Plateau Research, Chinese Academy of Sciences, Beijing, China

Correspondence to:

K. Henkel,
karoline.henkel@uni-jena.de

Citation:

Henkel, K., T. Haberzettl, G. St-Onge, J. Wang, M. Ahlborn, G. Daut, L. Zhu, and R. Mäusbacher (2016), High-resolution paleomagnetic and sedimentological investigations on the Tibetan Plateau for the past 16 ka cal B.P.—The Tangra Yumco record, *Geochem. Geophys. Geosyst.*, 17, doi:10.1002/2015GC006023.

Received 21 JUL 2015

Accepted 22 JAN 2016

Accepted article online 2 FEB 2016

Abstract The spatial distribution of paleomagnetic secular variation (PSV) records on the Tibetan Plateau and adjacent areas covering the Holocene and Late Glacial is sparse. In order to reconstruct PSV in this area, a piston core covering the past 17.5 ka cal B.P. retrieved from Lake Tangra Yumco, southern-central Tibetan Plateau, was analyzed. In the laminated sediments, several event layers are intercalated. Those were identified by sedimentological analysis and excluded for age-depth modeling and interpretation. Paleomagnetic measurements on u-channels reveal two contrasting core sections. The lower section (dated to 17.5–15.9 ka cal B.P.) is very coarse grained (up to 220 μm) and characterized by low intensities (0.8 mA m^{-1}) and high maximum angular deviation values (mean 25°), making it unsuitable for PSV reconstruction. In contrast, the upper unit (dated to <15.9 ka cal B.P.) yields ideal properties with a well-defined magnetization carried by low-coercivity minerals in the pseudo single domain state making those younger sediments a proper record for PSV studies. The robustness of the PSV reconstruction for the past 3000 years is highlighted by a comparable inclination and declination pattern of three short sediment cores (2 m) from Tangra Yumco. On a regional scale, the obtained inclination signal for the past 15.9 ka cal B.P. is in good agreement with the Lake Baikal record (3000 km to the North), PSV stack for East Asia, as well as with predictions of geomagnetic field models. This study is a step forward in constructing a PSV reference curve for central Asia.

1. Introduction

Paleomagnetic secular variations (PSV) describe the spatial and temporal behavior of the Earth's magnetic field during periods of stable magnetic polarity. For variations on time scales less than 5 years, an external origin is assumed, while PSV on longer time scales are of internal origin [Bloxham and Gubbins, 1985]. Besides the modeling of PSV for the past 400 years based on historical data mainly from naval and merchant ship logs [Jackson *et al.*, 2000], a globally increasing number of PSV records obtained from fired archeological material, volcanic rocks, and marine and lacustrine sequences allowed the development of global time-varying spherical harmonic models of the geomagnetic field over time spans of the past 3000, 7000, 9000, and 10,000 years based on a highly uneven spatial distribution of original records (CAL57k.2 [Korte and Constable, 2005], CAL53k.3 and ARCH3k.1 [Korte *et al.*, 2009], CAL510k.1b [Korte *et al.*, 2011], and pfmk.1b [Nilsson *et al.*, 2014b]).

In regions having numerous PSV records such as Europe and northern North America, Holocene PSV reconstructions provide insight on the behavior of the Earth's magnetic field, its impact on the cosmogenic nuclide production rates and can be used as a dating tool [Barletta *et al.*, 2010b; Snowball and Sandgren, 2002]. The use of magnetostratigraphy as a dating tool in Holocene paleoclimatic studies is becoming increasingly important in regions where the reliability of radiocarbon ages is limited. There, magnetostratigraphy allows strata to be correlated on a regional scale [Haberzettl, 2015; Haberzettl *et al.*, 2013; Ólafsdóttir *et al.*, 2013; St-Onge and Stoner, 2011; Yang *et al.*, 2009] and also absolutely dated by a comparison of a PSV record to the predictions of geomagnetic field models [Barletta *et al.*, 2010a]. However, the quality of the model predictions is limited by the spatial distribution of PSV records, their data quality, as well as by the quality of the chronologies of the contained records.

For central Asia, the density of PSV records covering the Holocene is very low (Figure 1a). This limits the reliability of geomagnetic field models in this area and further data are needed to test the accuracy of the

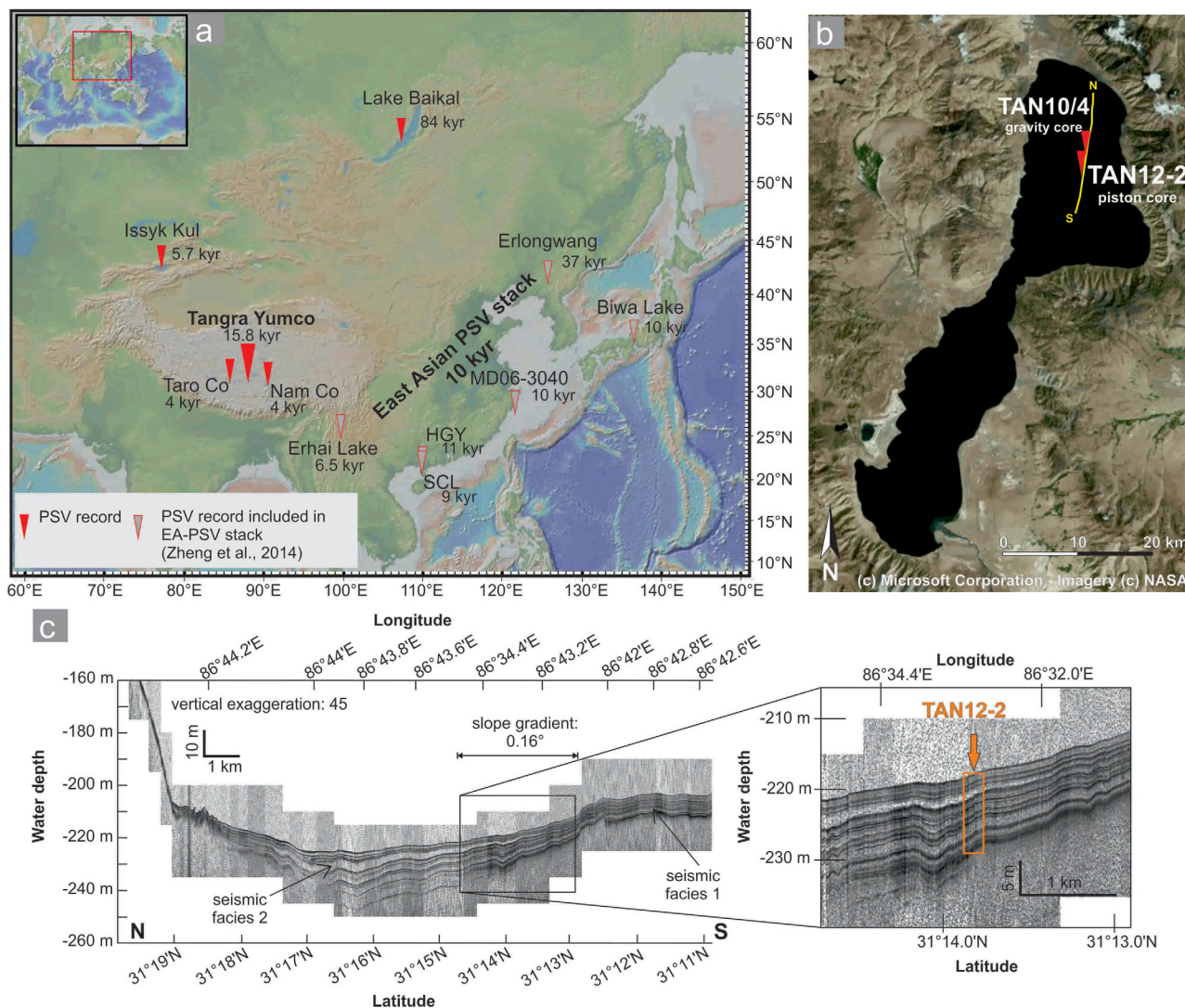


Figure 1. (a) Map of central Asia and adjacent areas with mentioned PSV records and their covered time span from lacustrine and marine sediments: Lake Baikal—*Peck et al.* [1996], Lake Biwa—*Ali et al.* [1999], Lake Erhai—*Hyodo et al.* [1999], Erlongwang maar lake—*Frank* [2007], Huguangyan maar lake (HGY)—*Yang et al.* [2012], Issyk Kul—*Gómez-Paccard et al.* [2012], MS06-3040—*Zheng et al.* [2014], Nam Co—*Kasper et al.* [2012], Shuangchilin maar lake (SCL)—*Yang et al.* [2009], Taro Co—*Haberzettl et al.* [2015], and Tangra Yumco—this study. Underlying map was created using <http://www.geomapp.org>. (b) Seismic line (yellow), coring locations of gravity core TAN10/4, and piston core TAN12-2 (satellite image: Microsoft Corporation—Imagery by NASA). (c) Part of the seismic profile of the lake bottom from N to S showing well-layered sediments of seismic facies 1 (hemipelagic sedimentation) and 2 (event layers) [*Akita et al.*, 2015]. Please note the 45 times vertical exaggeration of the seismic profile. The inset magnifies the coring position at a slope gradient of 0.16°.

models. On the Tibetan Plateau, no PSV records covering the Holocene were available until recently. In a first publication utilizing PSV data from the Tibetan Plateau, a 4000 year long radiocarbon-dated gravity sediment core from Lake Nam Co (Figure 1a) was validated by comparing the inclination and declination data to the predictions of geomagnetic field models [*Kasper et al.*, 2012]. A similar approach only using inclination data was also used for a 800 year long sediment core from the small TT-Lake [*Ahlborn et al.*, 2015]. In addition, the application of inclination data for stratigraphic correlation was successfully tested on several, individually radiocarbon-dated gravity cores spanning the past 4000 years from Lakes Taro Co and Tangra Yumco (Figure 1a) [*Haberzettl et al.*, 2015]. Although environmental magnetic studies of lacustrine sediments for longer time spans (i.e., the late Quaternary) are available [*Su et al.*, 2013a,b; *Zhu et al.*, 2003], no PSV records spanning the entire Late Glacial and Holocene have been published so far.

In order to close this gap of knowledge and to provide a base for further paleomagnetic investigations on the Tibetan Plateau, we present the first high-resolution PSV record covering the time since the Late Glacial from Lake Tangra Yumco, southern-central Tibetan Plateau. We compare the new PSV record with data sets

from Lake Baikal [Peck *et al.*, 1996], a stack for East Asia (EA stack) [Zheng *et al.*, 2014], and global geomagnetic field model predictions [Korte *et al.*, 2011; Nilsson *et al.*, 2014b] to assess the quality and accuracy of the new record.

2. Site Description

The terminal Lake Tangra Yumco (30°45'N–31°22'N, 86°23'E–86°49'E) with a surface area of 836 km² [Akita *et al.*, 2015] and a maximum water depth of 230 m [Haberzettl *et al.*, 2015] is one of the largest and the deepest lake on the Tibetan Plateau. The lake is located in an active N-S trending graben structure [Gao *et al.*, 2007] and consists of a shallower southern part (water depth >110 m) [Wang *et al.*, 2015] and a much deeper northern one (230 m) with steep slopes and a flat central basin (Figure 1b). Hydroacoustic surveys of the northern part reveal two contrasting seismic units. The first one shows continuous, parallel, and nearly horizontal reflectors with high amplitude interpreted as hemipelagic sedimentation. The second facies has low amplitude, is intercalated within the first facies (Figure 1c), and is interpreted as event layer sedimentation [Akita *et al.*, 2015].

Tangra Yumco sediments have been studied for paleoecological, paleohydrological, and paleoclimatic purposes in the recent years. Besides the analysis of lake level fluctuations in order to derive changes in the monsoon intensity [Ahlborn *et al.*, 2015; Miehe *et al.*, 2014; Rades *et al.*, 2013], a micropaleontological and sedimentological study described subaqueous mass movements [Akita *et al.*, 2015]. In gravity core TAN10/4, which forms the uppermost part of the record presented in this study, four graded sandy silt layers were classified as turbidites while a fifth sandy silt layer without grading was classified as a debrite [Akita *et al.*, 2015]. The pelagic sediments are the focus of this PSV study.

3. Material and Methods

3.1. Core Recovery and Composite Profile

Based on a seismic survey [Akita *et al.*, 2015] in the northern part of Tangra Yumco, the most promising position for coring undisturbed sediments was chosen (Figure 1c). The coring position was not at the deepest part of the lake, as thick sequences of event layers are common there (Figure 1c). Nevertheless, the coring position, located only 100 m west of the seismic profile, exhibits nearly horizontal reflectors (seismic facies 1, slope gradient 0.16° with intercalated event layers (seismic facies 2) and is not affected by faults mapped by Akita *et al.* [2015] (Figure 1c). During a field campaign in 2012, two Uwitec piston cores (TAN12-1, 2 m length and TAN12-2, 11.5 m length, inner diameter 90 mm) were retrieved from a water depth of 217 m almost at the same position (31°13.93'N, 86°43.25'E, Figure 1b). Unfortunately, it was not possible to obtain a parallel core to TAN12-2. As only one bore hole was used for the coring of TAN12-2, sediment from the base of each 2 m section contained in the core catcher is missing. These missing intervals are shown as 17 cm long sediment gaps in the composite profile. For a better handling, the 2 m long plastic core liners were cut in 1 m sections in the field.

Located 2 km north of the piston coring position, the well-investigated gravity core TAN10/4 (1.62 m length, 31°15.15'N, 86°43.37'E, 223 m water depth) exhibits a robust radiocarbon-based chronology and highlights the potential of lacustrine sediments of Tangra Yumco for environmental and magnetic reconstructions [Akita *et al.*, 2015; Haberzettl *et al.*, 2015]. Therefore, TAN10/4 was used to create a composite sediment profile because it has an undisturbed sediment-water interface. Piston core TAN12-1 has a disturbed and compacted surface, a common feature of surface piston cores resulting from the use of a ground plate. Piston core TAN12-2 misses the uppermost 13 cm of sediment. The composite profile was established by correlating gravity core TAN10/4 to piston core TAN12-2 based on lithology, magnetic susceptibility, and Ti profiles (Figure 2a).

3.2. Sedimentological Analysis

Sedimentological analyses were carried out in the laboratory of the department of *Physical Geography* of the Institute of Geography (Friedrich Schiller University Jena, Germany). Core sections TAN12-1 and TAN12-2 were split longitudinally and one half was digitally photographed and the lithology was described based on color, texture, grain size, and bedding structures. Magnetic susceptibility was measured with a surface scanning point sensor (type MS2E, Bartington Instruments Ltd) at 2 mm increments. XRF scanning and radiographic images were acquired with an ITRAX XRF core scanner [Croudace *et al.*, 2006] at 2 and 0.2 mm steps in the mm to sub-mm laminated sections.

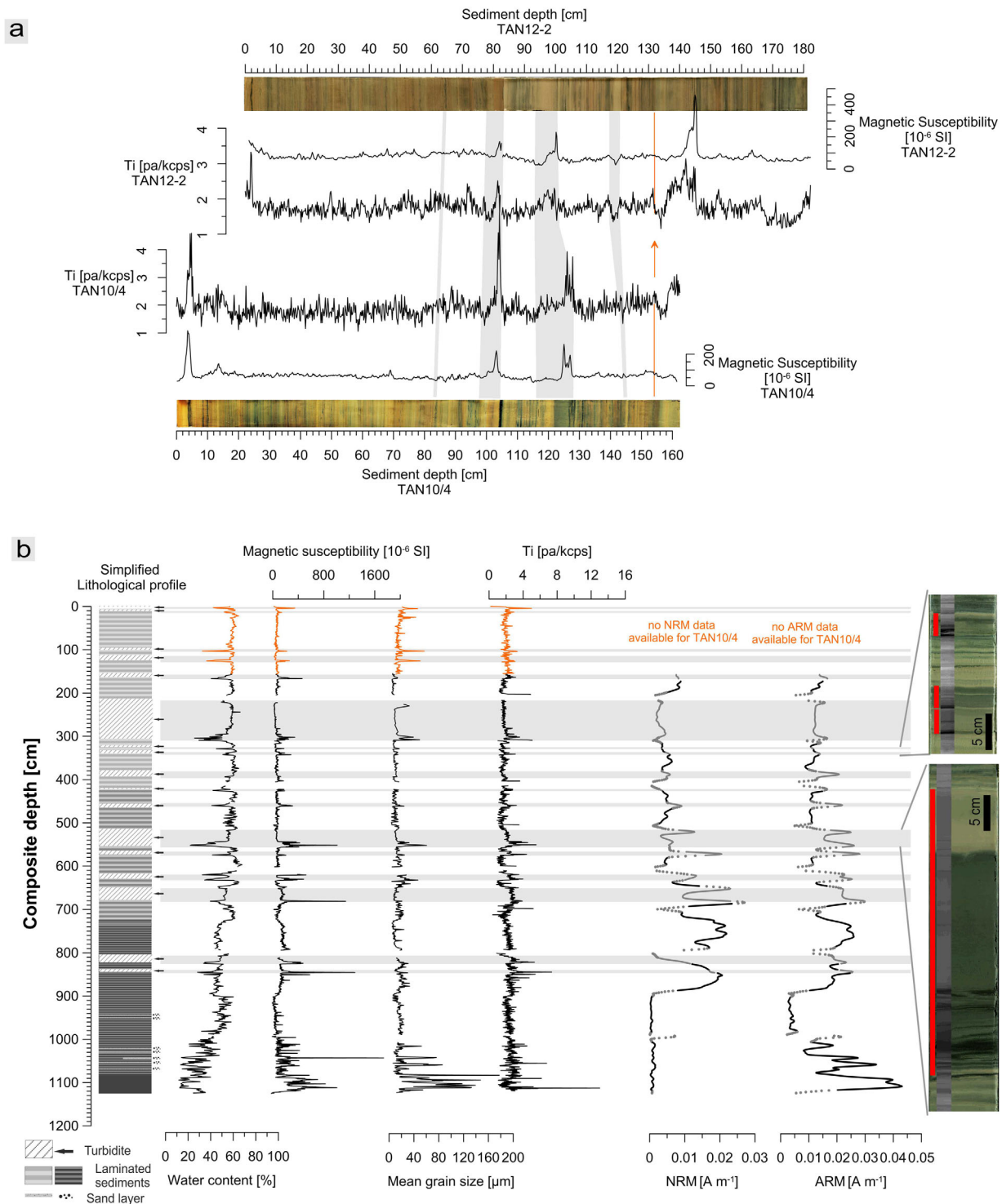


Figure 2. (a) Correlation of gravity core TAN10/4 with the upper two sections of TAN12-2 based on lithology, magnetic susceptibility, and Ti (peak area (pa) normalized by kilo counts per second (kcps)). Grey bars indicate identical horizons. The position chosen for a switch from TAN10/4 to TAN12-2 for a composite profile is indicated by the orange line. (b) Simplified lithology with water content, magnetic susceptibility, mean grain size, and Ti for TAN12-2 (black line) and TAN10/4 (orange line) which were used to detect event layers (gray bars). Core and radiographic images of some examples for event layers (red lines) are shown in the right including some hemipelagic sedimentation. NRM and ARM intensities are higher in the turbidites (grey lines). Edge effect affected data points from the top and bottom of each section as well as above and below event layers larger than 8 cm are shown as single data points.

Each core section was subsampled with one u-channel (u-shaped plastic liner of 2×2 cm cross section) and two double-L-channels [Nakagawa, 2007]. One of the double-L-channels was immediately subsampled in 1 cm intervals to determine the water content by weighing before and after freeze drying. For grain size

analysis, small sediment samples in 1 cm increments were taken and treated with 15%–30% hydrogen peroxide (H_2O_2) and 10%–15% hydrochloric acid (HCl) to remove organic matter and carbonates. After adding 5 mL sodium pyrophosphate ($\text{Na}_2\text{HPO}_4 \cdot \text{H}_2\text{O}$), the samples were shaken for 12 h to avoid microaggregates. The grain size measurement was carried out with a Laser Particle Size Analyzer (Beckman Coulter, LS 13320) in several 60 s cycles until a reproducible signal was obtained and the grain size distribution was calculated by applying the “Fraunhofer” optical model. The mean grain size was calculated using a modified version of the Gradistat 4.2 software [Blott and Pye, 2001].

3.3. Paleomagnetic Measurements

Paleomagnetic measurements on u-channels from TAN12-1 and TAN12-2 were performed at the *Institut des sciences de la mer de Rimouski* (ISMER) of the Université du Québec à Rimouski (UQAR), Canada. Natural remanent magnetization (NRM) was measured at 1 cm intervals using a 2G Enterprises™ 755 superconducting rock magnetometer (SRM) by applying a stepwise alternating field (AF) demagnetization at peak fields of 0–90 mT (0–60 mT in 5 mT increments, 60–90 in 10 mT increments). Fourteen demagnetization steps (5–80 mT) were selected to define the characteristic remanent magnetization (ChRM) by principal component analysis (PCA) [Kirschvink, 1980] using an Excel spreadsheet [Mazaud, 2005], which also determines the median destructive field (MDF) and the maximum angular deviation (MAD). MAD values are used to assess the quality of the directional record, where values lower than 5° are considered to be high-quality paleomagnetic data [Stoner and St-Onge, 2007]. According to the response function of the three SQUID coils, a smoothing effect over several centimeters occurs [Weeks et al., 1993]. Therefore, the data of the top and basal 5 cm of each section are excluded from interpretation. However, as the MAD values describe a similar data quality for the edge effect affected intervals compared to the nonaffected, the paleomagnetic data are shown as dots (data points) to reduce data gaps due to piston coring. As the cores were not azimuthally oriented during coring, declination data are relative. Sections were fitted together using the data unaffected by the edge effect. Subsequently, the resulting mean declination was set to zero.

An anhysteretic remanent magnetization (ARM) was acquired in a 100 mT AF superposed with a direct current (DC) bias field of 0.05 mT. Additionally, an isothermal remanent magnetization (IRM) and a saturated isothermal remanent magnetization (SIRM) were acquired applying a DC bias field of 0.3 and 0.95 T with a pulse magnetizer module. After each step, the ARM, IRM, and SIRM were demagnetized and measured with the same AF demagnetization steps as for NRM (ARM and IRM to 70 mT and SIRM to 80 mT).

Hysteresis loops and remanence curves were measured on 18 subsamples with an alternating gradient force magnetometer (Princeton Measurements Corp., MicroMag model 2900). The magnetization saturation (M_s), coercive force (H_c), saturation remanence (M_{rs}), and coercivity of remanence (H_{cr}) were extracted from the hysteresis loops. To characterize the magnetic mineralogy and magnetic domain state, the ratios M_{rs}/M_s and H_{cr}/H_c were plotted against each other [Day et al., 1977].

On gravity core TAN10/4, only AF demagnetization steps from 5 to 100 mT were carried out for NRM measurements. But as the NRM without an AF demagnetization (0 mT) was not measured, no MDF data are available. Further details can be found in Haberzettl et al. [2015].

3.4. Age-Depth Modeling

For the chronology of the composite profile consisting of gravity core TAN10/4 and piston core TAN12-2, radiocarbon ages from gravity core TAN10/4 [Haberzettl et al., 2015] and piston core TAN12-2 were combined. Bulk sediment samples were used for radiocarbon dating (Beta Analytic Inc., USA), as except for one piece of wood, no plant macro remains were available. The samples for radiocarbon dating were selected carefully to avoid dating sections containing event layers with potentially reworked material. In total, six radiocarbon ages for gravity core TAN10/4 and 22 radiocarbon ages for piston core TAN12-2 were obtained (Table 1). To determine the modern reservoir effect, material of a growing water plant, as well as the sediment-water interface of two gravity cores retrieved in 2010 and 2011 were dated [Haberzettl et al., 2015]. The conventional radiocarbon age of the water plant was used as the reservoir effect. Assuming a constant reservoir effect over time, the reservoir effect was subtracted from the ^{14}C ages, except for the dated piece of (terrestrial) wood. Subsequently, the ages were calibrated with the online version of the software Calib 7.0 [Stuiver and Reimer, 1993], applying the IntCal13 data set [Reimer et al., 2013] to calculate calibrated median ages and 2σ errors. A reservoir effect is often observed in hardwater lakes, as weathered

Table 1. Radiocarbon Ages for TAN10/4 and TAN12-2

Lab Number	Section	Section Depth (cm)	Composite Depth (cm)	ECCD (Event Corrected Composite Depth) (cm)	Conventional Radiocarbon Age (B.P.)	Error (year)	Reservoir Corrected Radiocarbon Age (B.P.)	Reservoir Corrected Calibrated Median Age (cal B.P.)	Reservoir Corrected Calibrated Min Age (cal B.P.)	Reservoir Corrected Calibrated Max Age (cal B.P.)
289070 ^a	Modern water plant ^b				2,070 ^b	40				
291393 ^a	TAN10/1	Surface	0	0	2,200	30		-60	-60	-60
295002 ^a	TAN10/4 ^{c,d}	Surface	0	0	2,140	30		-60	-60	-60
295003 ^a	TAN10/4	24	24	16	3,450	40	1,380	1,300	1,260	1,370
295004 ^a	TAN10/4 ^{c,d}	41	41	33	3,410	40	1,340	1,270	1,220	1,320
382663 ^a	TAN10/4	78	78	70	4,940	30	2,870	2,990	2,920	3,080
295005 ^a	TAN10/4 ^{c,d}	115.5 (wood)	115.5	101	2,480	30	2,480	2,580	2,430	2,720
295006 ^a	TAN10/4 ^{c,d}	152	152	124	5,260	40	3,190	3,420	3,340	3,480
343267	TAN12-2-2 ^{c,d}	82	186	148	5,410	30	3,340	3,580	3,540	3,640
343268	TAN12-2-4 ^{c,d}	13	323	198	6,510	40	4,440	5,050	4,880	5,080
343269	TAN12-2-4 ^{c,d}	89	399	249	7,160	40	5,090	5,820	5,740	5,920
348504	TAN12-2-5 ^{c,d}	23	437	283	7,920	40	5,850	6,670	6,550	6,750
340279	TAN12-2-5 ^c	49	463	301	8,920	40	6,850	7,680	7,610	7,760
348505	TAN12-2-5	77	491	329	9,370	40	7,300	8,100	8,020	8,180
343270	TAN12-2-6 ^{c,d}	70	576	365	9,030	40	6,960	7,790	7,690	7,870
348506	TAN12-2-6 ^{c,d}	94	600	389	10,660	40	8,590	9,540	9,490	9,630
343271	TAN12-2-7 ^{c,d}	33	643	419	11,080	40	9,010	10,200	10,150	10,250
348507	TAN12-2-7 ^{c,d}	74	684	430	11,870	50	9,800	11,220	11,150	11,290
382664	TAN12-2-8	14	714	460	12,470	40	10,400	12,270	12,070	12,420
382665	TAN12-2-8	24	724	470	13,350	40	11,280	13,130	13,060	13,220
348508	TAN12-2-8	29	729	475	13,210	50	11,140	13,020	12,850	13,100
340280	TAN12-2-8 ^{c,d}	71	771	517	12,360	50	10,290	12,070	11,930	12,240
348509	TAN12-2-8 ^c	93	793	539	13,620	50	11,550	13,390	13,280	13,470
343272	TAN12-2-9 ^c	27	828	560	13,700	60	11,630	13,460	13,330	13,570
382666	TAN12-2-9	48	849	574	14,850	40	12,780	15,220	15,080	15,380
382667	TAN12-2-9 ^{c,d}	65	865	590	13,730	40	11,660	13,500	13,420	13,570
348510	TAN12-2-9 ^{c,d}	84	885	610	15,170	60	13,100	15,720	15,430	15,970
329516	TAN12-2-10 ^{c,d}	10	904	629	15,490	60	13,420	16,150	15,920	16,350
329517	TAN12-2-10 ^{c,d}	92	986	711	16,120	70	14,050	17,080	16,790	17,370
340281	TAN12-2-11 ^{c,d}	87	1,078	803	16,310	70	14,240	17,340	17,100	17,560

^aHaberzettl et al. [2015].
^bUsed as reservoir effect.
^cUsed for chronology1.
^dUsed for chronology2.

carbonatic bedrock of the drainage basin alters the radiocarbon ages. For the chronology, an age-depth model was established by applying a linear interpolation between the youngest median ages in stratigraphic order.

4. Lithology

In total, the composite profile of Tangra Yumco has a length of 1124 cm and consists of fine-grained silty sediments with well-preserved laminations ranging from several mm to sub-mm. The total organic carbon (TOC) content is generally very low (0.1–1.2%; M. Ahlborn, unpublished data, 2015). The sediment color changes from black in the lower part (1124–800 cm) to bright yellow-brownish in the upper part (515–0 cm) with a transition zone of yellow-brownish and dark-grayish laminations (800–515 cm) (Figure 2). Especially in the lower blackish part, sand layers with decreasing thickness from 1084 to 900 cm are observed. Intercalated in the laminated sediments (correlating with seismic facies 1) are intervals of homogenous silty sediments of varying thicknesses (centimeter up to nearly 1 m, correlating with seismic facies 2). The latter are regarded as reworked material of single events that were recognized in earlier investigations of the Tangra Yumco sediments and classified in most cases as turbidites [Akita et al., 2015]. As not all event layers in TAN12-2 meet the requirements for turbidites, we will use the more general term event layer. Compared to the laminated hemipelagic sedimentation, event layers can be identified by their homogenous lithology, lower water content, higher magnetic susceptibility, and a mainly coarser grain size at the base associated with grading (Figure 2). These parameters were used to further detect thinner event layers and exclude them from age-depth modeling. The top of clearly identifiable event layers is characterized by changes in

lithology from homogenous to laminated sediments and simultaneous changes in the Ti content. There are no hints of an erosion of previously deposited laminated sediments, as no erosional features at the base of turbidites are visible. In total, 19 event layers with thicknesses from 2 to 84 cm could be distinguished and an event corrected composite depth (ECCD) profile with a length of 849 cm was established. The well-preserved laminated sediments which are regarded as hemipelagic sedimentation show no signs of intense bioturbation or sediment mixing and are therefore ideal archives for paleomagnetic, paleoenvironmental, and paleoclimatic studies.

Detected event layers correspond to high NRM and ARM intensities (Figure 2b) indicating that the magnetic concentration, grain size, and mineralogy are significantly different from the hemipelagic sedimentation. Although *Haberzettl et al.* [2015] noticed, that thinner (4–14 cm) event layers observed in TAN10/4 do not affect the inclination and declination, a smoothing error influencing magnetic parameters as well as a flattening of the inclination cannot be excluded [*St-Onge et al.*, 2004]. Therefore, 5 cm intervals above and below event layers of a thickness greater than 8 cm have to be discussed with care and will also be handled as edge effect affected (Figure 2). Magnetic measurements in event layers thinner than 8 cm thickness are mostly influenced by the hemipelagic sedimentation, so that the influence of event layers on the magnetic parameters can be neglected due to the smoothing effect.

5. Chronology

The application of the age of the modern water plant (2070 ± 40 B.P.) [*Haberzettl et al.*, 2015] as reservoir effect instead of bulk sediment samples from the sediment-water interface is reasonable, as no age averaging over 1 cm bulk sediment occurs. Nevertheless, the age of the modern water plant in the same range as the dated bulk sediment samples from the sediment-water interface from two gravity cores (2200 ± 30 and 2140 ± 40 B.P.) [*Haberzettl et al.*, 2015] confirming the use of the modern water plant for reservoir correction. The reliability of the reservoir effect was also tested with the uncorrected radiocarbon age of a wood sample (2480 ± 30 B.P.) [*Haberzettl et al.*, 2015]. This age fits in a linear interpolation of the youngest median ages in stratigraphic order [*Haberzettl et al.*, 2015]. In addition, optically stimulated luminescence (OSL) ages on the gravity core yield an age offset of 2000 years to the uncorrected radiocarbon ages [*Long et al.*, 2015]. Therefore, the assumption of a constant reservoir effect over time seems to be reasonable.

In a first iteration, the linear interpolation between the youngest ages in stratigraphic order resulted in unreasonable increased sedimentation rates in two intervals (Chronology1, dashed line in Figure 3). This appears to be an artifact of this modeling approach as no changes in lithology can explain the increased sedimentation rates. Therefore, two further apparently too old ages were excluded in a second iteration (Chronology2, Figure 3) consisting of the remaining 18 radiocarbon ages (Table 1). The sedimentation rate of 3.6 mm a^{-1} in the lower part of the core (ECCD 848–711 cm, 17.5–17.1 ka cal B.P.) is 6 times higher than in the upper part (0.6 mm a^{-1} , ECCD 711–0 cm, 17.1–0 ka cal B.P.).

6. Paleomagnetic Investigations

6.1. Magnetic Parameters

The event corrected composite of core TAN12-2 can be divided into two sections based on its magnetic properties and NRM intensities (Figures 4a and 5). The lower section A (ECCD 848–618 cm, 17.5–15.9 ka cal B.P.) is characterized by a very unstable NRM demagnetization (Figure 4a) and very low NRM intensities (mean = 0.8 mA m^{-1} , Figure 5e). In contrast, NRM intensities in the sediments in section B (ECCD 617–0 cm, <15.9 ka cal B.P.) are 10 times higher (mean = 8.3 mA m^{-1}) and the AF demagnetization exhibits a stable single-component magnetization (Figure 4a) (Z-plots) [*Zijderveld*, 1967].

The separation in two sections is visible in further parameters reflecting changes in concentration such as the ARM and SIRM [*Stoner and St-Onge*, 2007] (Figure 5). In section A (ECCD 848–618 cm), ARM values are high and show large variations ($8.1\text{--}43.0 \text{ mA m}^{-1}$, mean = 23.2 mA m^{-1}) below ECCD 731 cm and are the lowest in the record between ECCD 730 and 626 cm (3.6 mA m^{-1}). In section B, the ARM is constant ($8.7\text{--}26.0 \text{ mA m}^{-1}$, mean = 15.7 mA m^{-1}). Similarly, the SIRM follows the same pattern with large variations

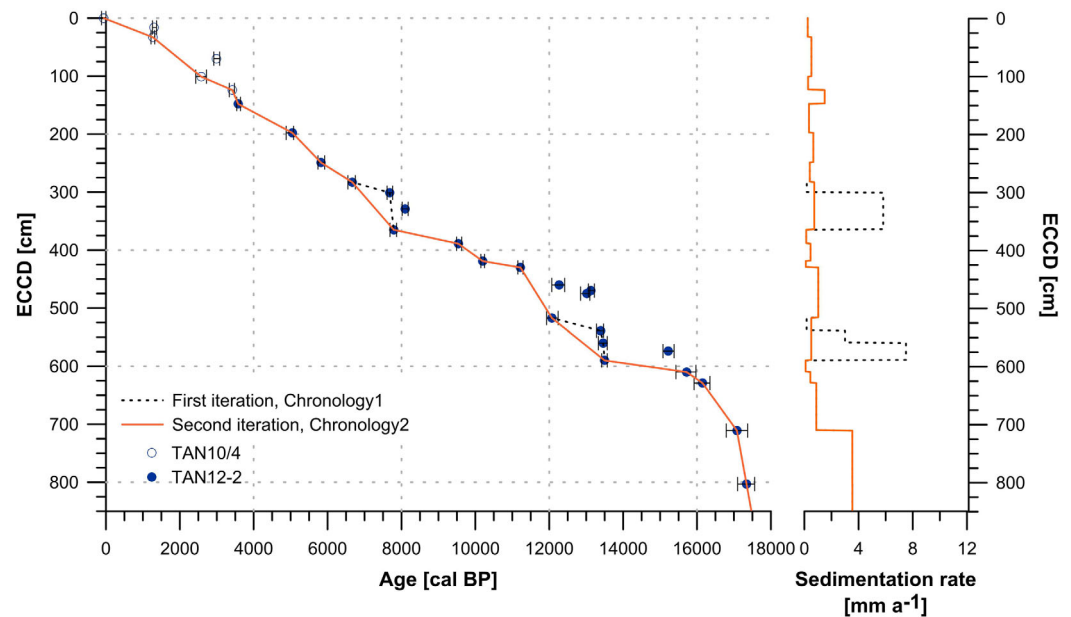


Figure 3. Age-depth model and sedimentation rates for the event corrected composite depth (ECCD) profile of Tangra Yumco consisting of gravity core TAN10/4 for the upper 1.5 m and piston core TAN12-2. As very high sedimentation rates were calculated in some parts of Chronology1 (dashed line) without any lithological evidence, two further ages were regarded as too old and excluded from Chronology2 (orange line).

below ECCD 731 cm ($0.27\text{--}2.38 \text{ mA m}^{-1}$), low values between ECCD 730 and 626 cm (mean = 0.15 mA m^{-1}), and are constant in section B (1.12 mA m^{-1}).

The coercivity of the sediments reflecting changes in the magnetic grain size and mineralogy is described by the Median Destructive Field (MDF) of the NRM (Figure 5c) [Stoner and St-Onge, 2007]. In section A, high amplitude variations ($3.7\text{--}72.8 \text{ mT}$) are observed compared to section B, where constant values are observed ($22.7\text{--}27.5 \text{ mT}$, Figure 5c). This stable MDF suggests that the mineral component and grain size carrying the NRM has not changed significantly. The mean MDF value of 26 mT in section B is consistent with a low-coercivity mineral such as magnetite as the carrier of the NRM, while amplitude variations seen in section A indicate changing proportions of low-coercivity and high-coercivity minerals.

This difference in sections A and B is also seen in the “pseudo S-ratio” (IRM/SIRM ratio, Figure 5i) that describes the relative contribution of low-coercivity to high-coercivity minerals [Stoner and St-Onge, 2007]. Except for the interval between ECCD 760 and 730 cm, the S-ratio of the TAN12-2 record is constant and high (mean = 0.9), illustrating the presence of lower-coercivity ferrimagnetic minerals like magnetite or titanomagnetite [Stoner and St-Onge, 2007]. Low-coercivity minerals as the main carrier of the NRM in the pseudo single domain state (PSD) are identified in the ratios M_{rs}/M_s and H_{cr}/H_c (Day plot, Figure 6) for section B, while in section A, the multidomain state dominates [Day et al., 1977]. Hysteresis loops also identify magnetite as the main magnetic carrier in section B (Figure 4b). The absence of a gyromagnetic magnetization acquisition at higher AF demagnetizations points to an absence of magnetic iron sulfides such as greigite (Figure 4a).

6.2. Paleomagnetic Secular Variations

Based on the high amplitude variations in the discussed parameters, sediments from section A seem to be a poor recorder of the paleomagnetic field. This is further supported by high MAD values (mean = 25.0°), assessing the poor quality of the directional data derived by PCA. Furthermore, unrealistic declination jumps (Figure 5b) and negative inclination values implying unlikely short-term geomagnetic reversals/excursions (Figure 5a) disprove the recording of PSV in section A.

In contrast, sediments in section B meet the criteria setup to assess the quality of sediments as recorder of geomagnetic field changes [Stoner and St-Onge, 2007; Tauxe, 1993]. Reliable PSV recording is supported by

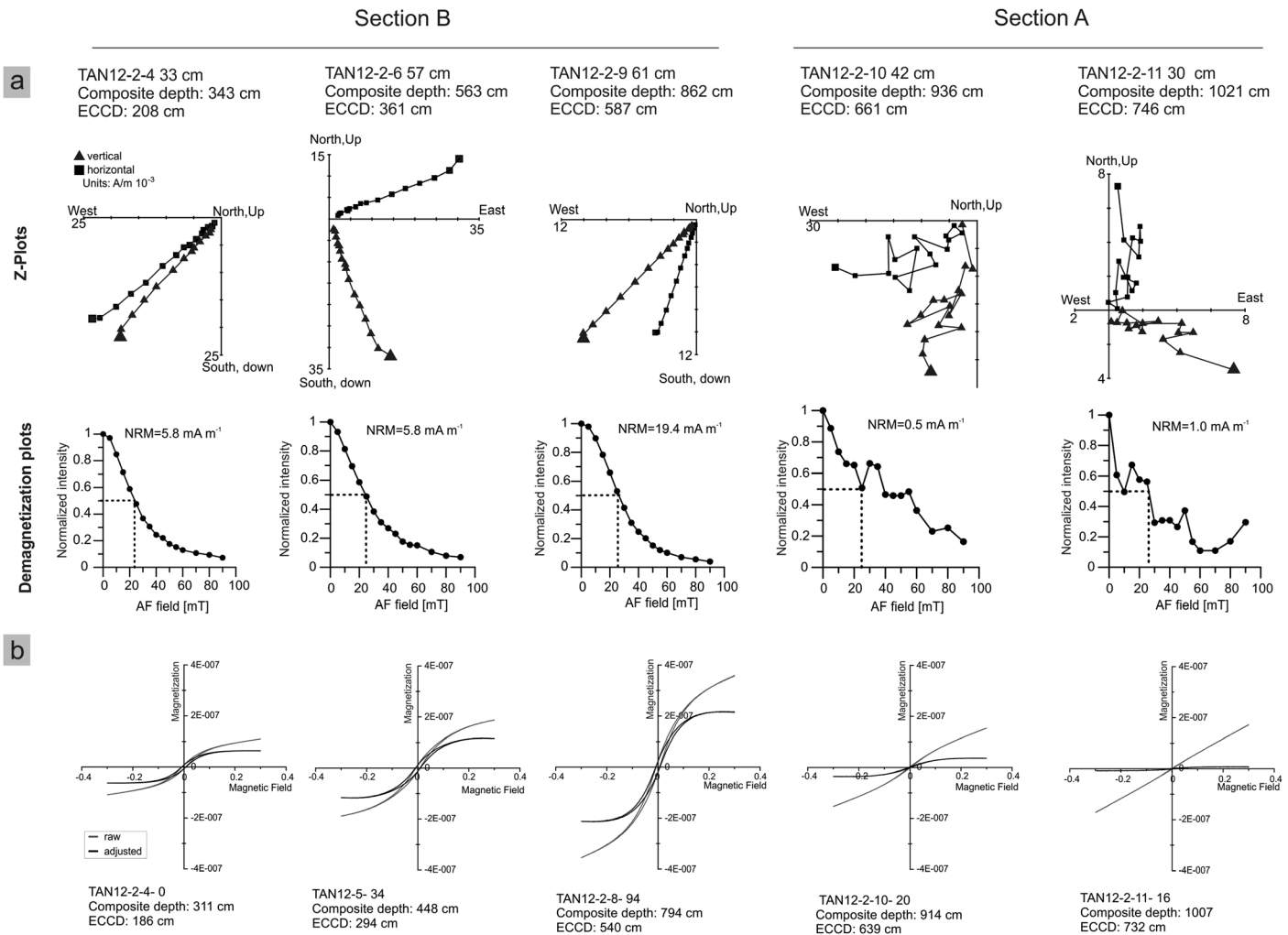


Figure 4. (a) AF demagnetization behavior of representative samples from sections A and B. Sample ID represents TAN12-2-“core section”-“sediment depth.” (top row) Z-plots [Zijderveld, 1967]. (bottom row) The corresponding normalized intensity decay during the AF demagnetization is displayed. The dashed lines represent the median destructive field (MDF). (b) Hysteresis loops of selected samples.

a strong and stable single-component magnetization (Figure 4a), MAD values below 5° (Figure 5d, mean = 1.57° without edge affected intervals), constant and stable magnetic mineralogy dominated by low-coercivity minerals, and by changes in concentration much lower than 1 order of magnitude (Figure 5c). The inclination in section B oscillates around the expected geocentric axial dipole (GAD = 50.4°) for the latitude of Tangra Yumco (Figure 5a). Nonetheless, a slightly shallower mean of 43.6° is observed.

A flattened inclination compared to the GAD, as it is observed in TAN12-2, is often noticed in marine and lacustrine sediments [Anson and Kodama, 1987; Frank, 2007]. Inclination shallowing can be explained by sedimentation processes such as pore water motions and compaction, which affect the detrital minerals carrying the ChRM [e.g., Bressler and Elston, 1980; Tauxe et al., 2008]. Especially, the compaction is believed to affect inclination [Anson and Kodama, 1987; Tauxe et al., 2008].

Declination in section B varies over 82° (Figure 5b). The declination is relative and the individual sections were rotated to fit the declination (the top of the section below was adjusted to the bottom of the section above, without respecting the edge effect affected ends). This correction might have resulted in an overarching declination trough with easterly directions at the bottom and top of section B and a westward swing between 325 and 280 cm ECCD. Further jumps in the declination occur due to event layer corrections. The trend of the edge effect affected intervals at the top and bottom of each section are clearly artifacts of the paleomagnetic measurements. It remains to be explained why declination is much more sensitive to the edge effect than inclination.

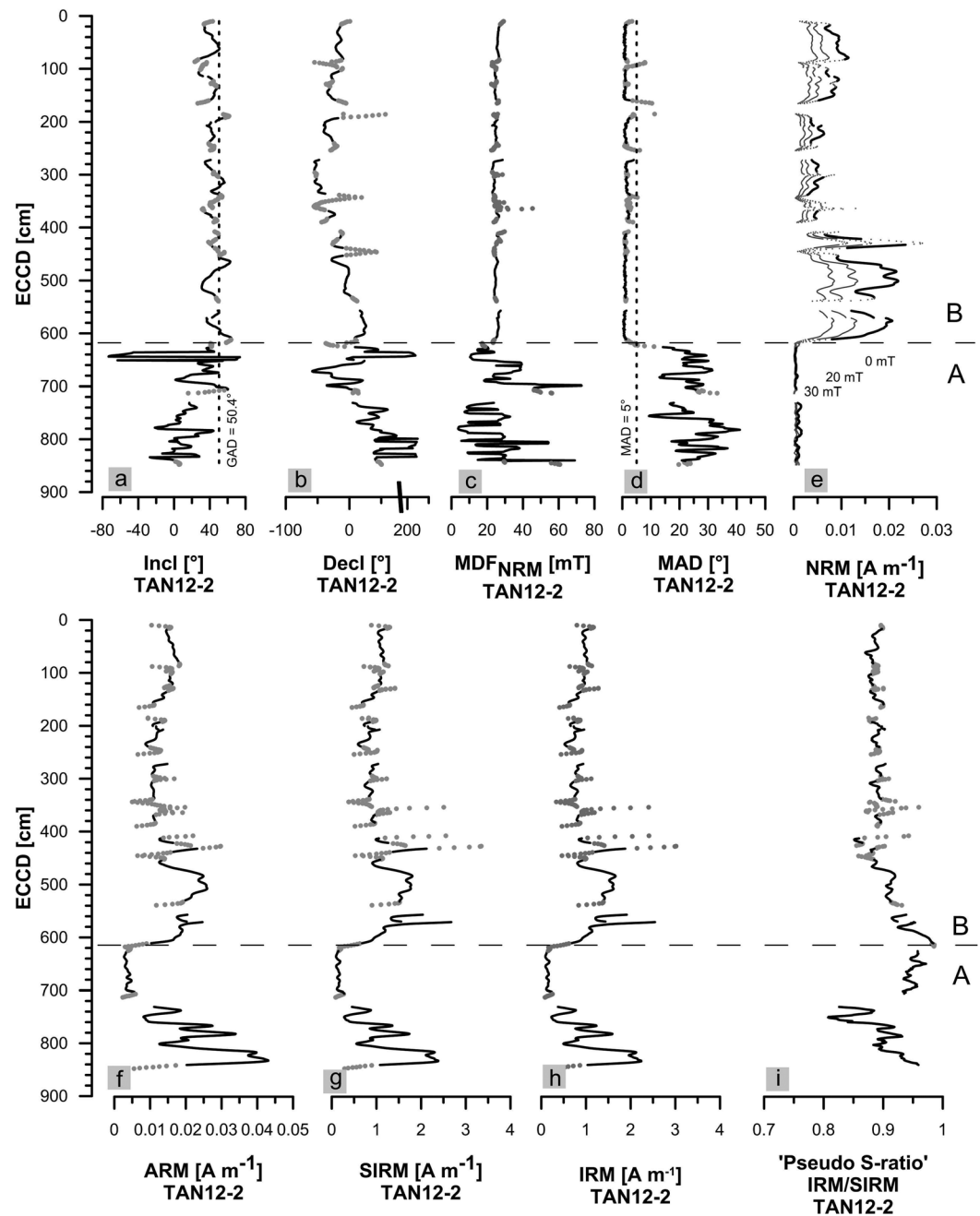


Figure 5. (a–i) Magnetic properties of piston core TAN12-2 on an event corrected composite depth (ECCD). The event corrected data obtained from the uppermost sections of TAN12-2 are shown instead of gravity core TAN10/4, as no NRM measurements were carried out on TAN10/4. Data affected by an edge effect caused by an event layer or core section break are displayed as data points (dots). Data gaps are due to sediment loss during piston coring. According to the NRM intensities, the record is divided into sections A and B. Please note the axis break in declination.

7. Intralake and Regional Comparison of Directional Records

7.1. Intralake Comparison of Directional Records

In a first paleomagnetic study on gravity cores from Tangra Yumco, a good preservation of the inclination was demonstrated for the upper 1.7 m [Haberzettl *et al.*, 2015]. To test whether the same signals are preserved in the piston cores, we compare the natural remanent magnetization as well as the directional record of the upper 2 m from TAN12-1 and TAN12-2 with gravity core TAN10/4 (Figure 7). As a chronological support for piston cores TAN12-1 and TAN12-2 is missing, all data are plotted on the individual depth

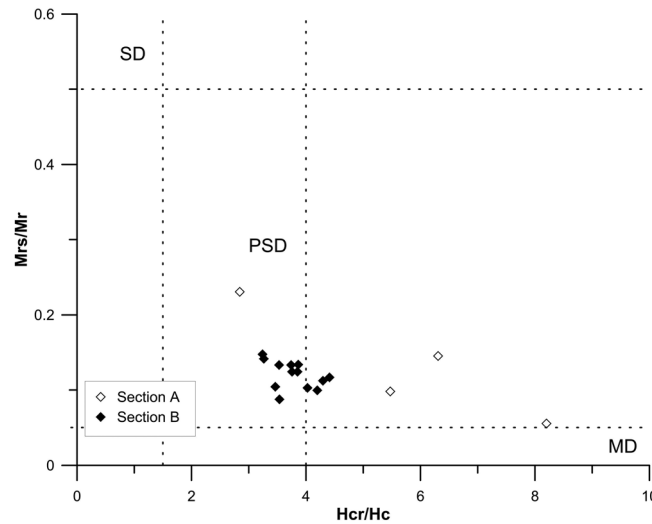


Figure 6. Day plot [Day et al., 1977] for samples from sections A and B from TAN12-2 illustrating that samples from section A are predominantly in the MD range while samples from section B are mainly composed of PSD grains. SD = single domain, PSD = pseudo single domain, and MD = multidomain.

scale with the event layers. A high quality of the magnetic measurements is exhibited by the low MAD values ($<5^\circ$) and MDF values ranging between 20 and 30 mT, suggesting low-coercivity minerals such as magnetite as the main carrier of the NRM.

The inclinations for TAN12-1, TAN12-2, and TAN10/4 are slightly shallower than the GAD prediction, which might be an effect of compaction. Both piston cores TAN12-1 and TAN12-2 yield an inclination pattern similar to the well-investigated TAN10/4 (Figure 7). Offsets in the location of single patterns like I4 (Figure 7) result from the presentation on individual core depth scales. The declination in the lower part of the piston cores is very similar and related structures can also be

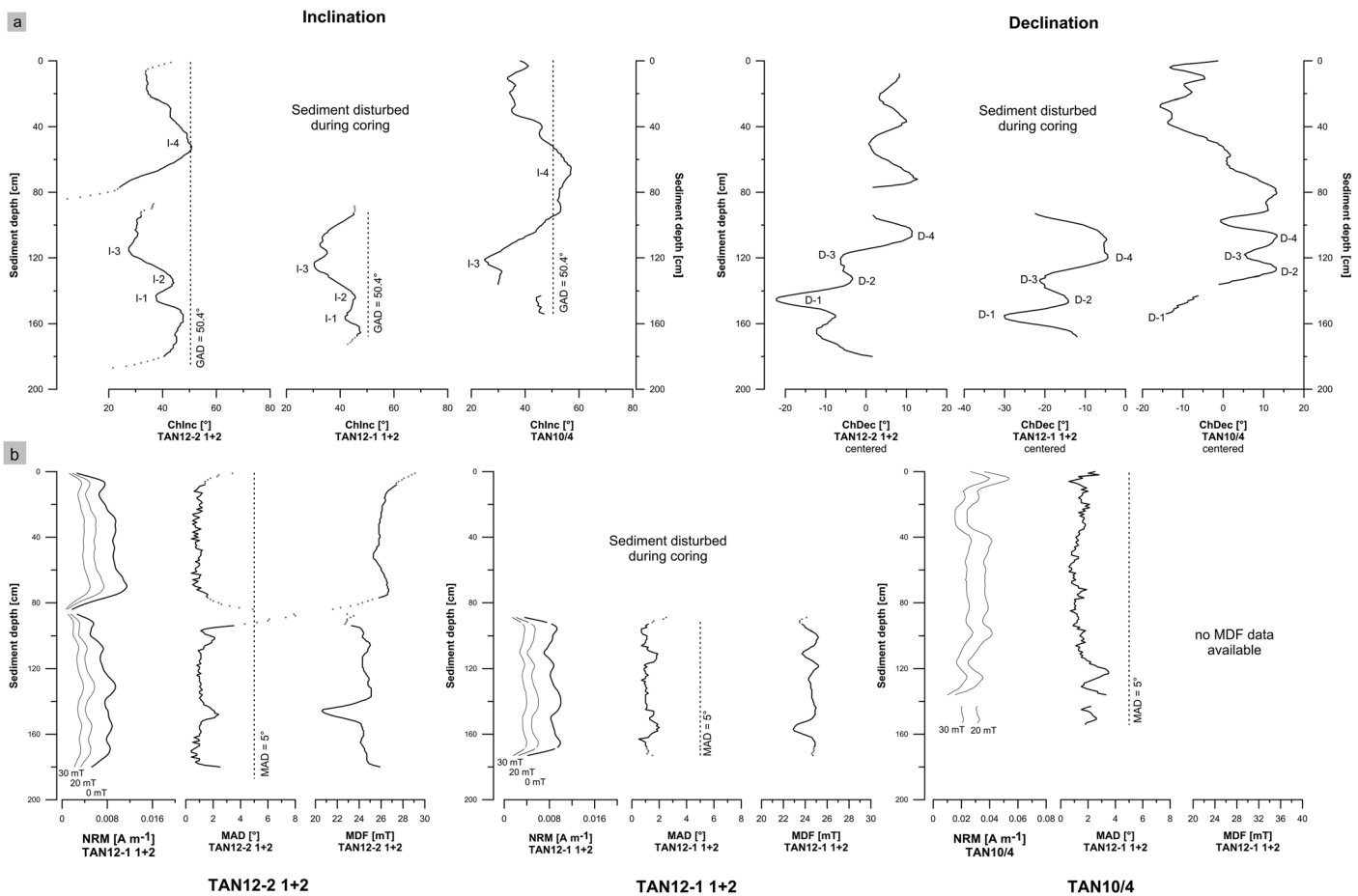


Figure 7. (a) Comparison of inclination and relative declination for piston cores TAN12-1 sections 1 + 2, TAN12-2 sections 1 + 2, and gravity core TAN10/4 on individual depth scales. In edge effect affected intervals, only the data points are shown. (b) Magnetic parameters including NRM intensities at demagnetizations of 0, 20, and 30 mT, MAD and MDF values.

found in gravity core TAN10/4. Due to the coring disturbance in the upper part of the piston cores, a comparison in the upper part is not possible. The good correlation of the declination in the piston cores is surprising, as the comparison of declination obtained from gravity cores in a study by *Haberzettl et al.* [2015] did not yield similar structures in the declination pattern. Nevertheless, the good match of the inclination in both piston cores as well as the gravity core highlights the good properties for paleomagnetic recording in the sediments of Tangra Yumco, the robustness of the measured inclination, and also confirms the use of TAN10/4 as top of the composite profile.

7.2. Inclination Comparison With Geomagnetic Field Models

Two families of models are available both based on geological, archeological, and sedimentary PSV data from the GEOMAGIA50 database [*Korhonen et al.*, 2008]. The CALS10K.1b model spanning the past 10 ka is based on recently refined modeling strategies of *Korte and Constable* [2005]. This method leads to a robust, but low-resolution prediction limited to temporal resolution estimations of around 500 years at individual locations [*Korte et al.*, 2011]. Based on a different modeling approach, a new family of field models was established spanning the past 9 ka (pfm9k) [*Nilsson et al.*, 2014b]. By comparing the obtained model with predictions from a preliminary model, age adjustments on individual chronologies were carried out [*Nilsson et al.*, 2014b] in an alternative way to *Korte et al.* [2011] to extract more information from the sedimentary PSV data.

A similarity in the inclination patterns between Tangra Yumco and both model predictions can be observed and several features like the multip peaked H7 can be correlated (Figure 8a). Especially in the early Holocene, the timing of H5-1 and L5 reveal only minor age offsets of <250 years (Figure 9). Unfortunately, the inclination maximum H6 could not be clearly defined in Tangra Yumco. In the late Holocene, the modeled inclination features are observed nearly up to 840 years earlier than at Tangra Yumco (L7, H8; Figures 8a and 9). This low potential for the application of model predictions for the past 5.7 and 4 kyr was previously recognized [*Gómez-Paccard et al.*, 2012; *Haberzettl et al.*, 2015]. Nevertheless, the similarity of the inclination pattern for the past 3000 years (disregarding the age offset) and the good comparability for the Holocene beyond 3000 years generally validates the model predictions, although age uncertainties need further clarification.

7.3. Inclination Comparison With Lake Baikal and East Asia PSV Stack

To check the reliability and reproducibility of the PSV record from Tangra Yumco, two further records were chosen for evaluation. Lake Baikal (84 kyr) [*Peck et al.*, 1996] and a PSV stack for East Asia (10 kyr) [*Zheng et al.*, 2014] (Figure 1a) are the closest available records comparable to our high-resolution PSV record in terms of the covered time frame, reliability of chronologies, and quality of the PSV record.

The comparison of PSV records is highly dependent on the quality of the individual chronologies. For the compilation of the EA stack, all data were interpolated in a temporal resolution of 20 years. Therefore, the PSV ages of the EA stack are constrained by ^{14}C ages with limited errors [*Zheng et al.*, 2014]. As four of six records implemented in the EA stack are based on discrete sample measurements, a high accuracy is reached [*Zheng et al.*, 2014]. In Lake Baikal, discrete sampling at 2 cm intervals gives a detailed record although only a low temporal resolution of 130 years per data point is reached for the shown time interval. A nearly linear age-depth relationship for the past 23 ka cal B.P. (sedimentation rate 0.11 mm a^{-1}) at Lake Baikal is based on reservoir corrected (surficial sediments, 1220 ^{14}C years) radiocarbon ages [*Peck et al.*, 1996].

Although distant (Figure 1a, Lake Baikal: 3000 km, single records of the EA stack: 1400–4600 km), the directional patterns of Tangra Yumco can be found in both records (Figure 8a, comparable inclination highs (H8-H1) and lows (L8-L1)). For the earliest part from 15.9 to 10.0 ka cal B.P., only a comparison with Lake Baikal is possible. The pattern in this time frame shows similar features between both records but the inclination low L2 is up to 900 years older in Lake Baikal (Figure 9). Additionally, the inclination decrease between H1 and L1 in Tangra Yumco is more abrupt in Lake Baikal (Figure 8a). Large temporal offsets still dominate the comparison with Tangra Yumco till 5.5 ka cal B.P., but get smaller for H6 and following inclination features (Figures 8a and 9).

Similar large and small-scale inclination patterns could be matched between Tangra Yumco and the EA stack for the Holocene (Figure 8a). Especially between 8.5 and 6.0 kyr (L4 to L5), distinctive features like the

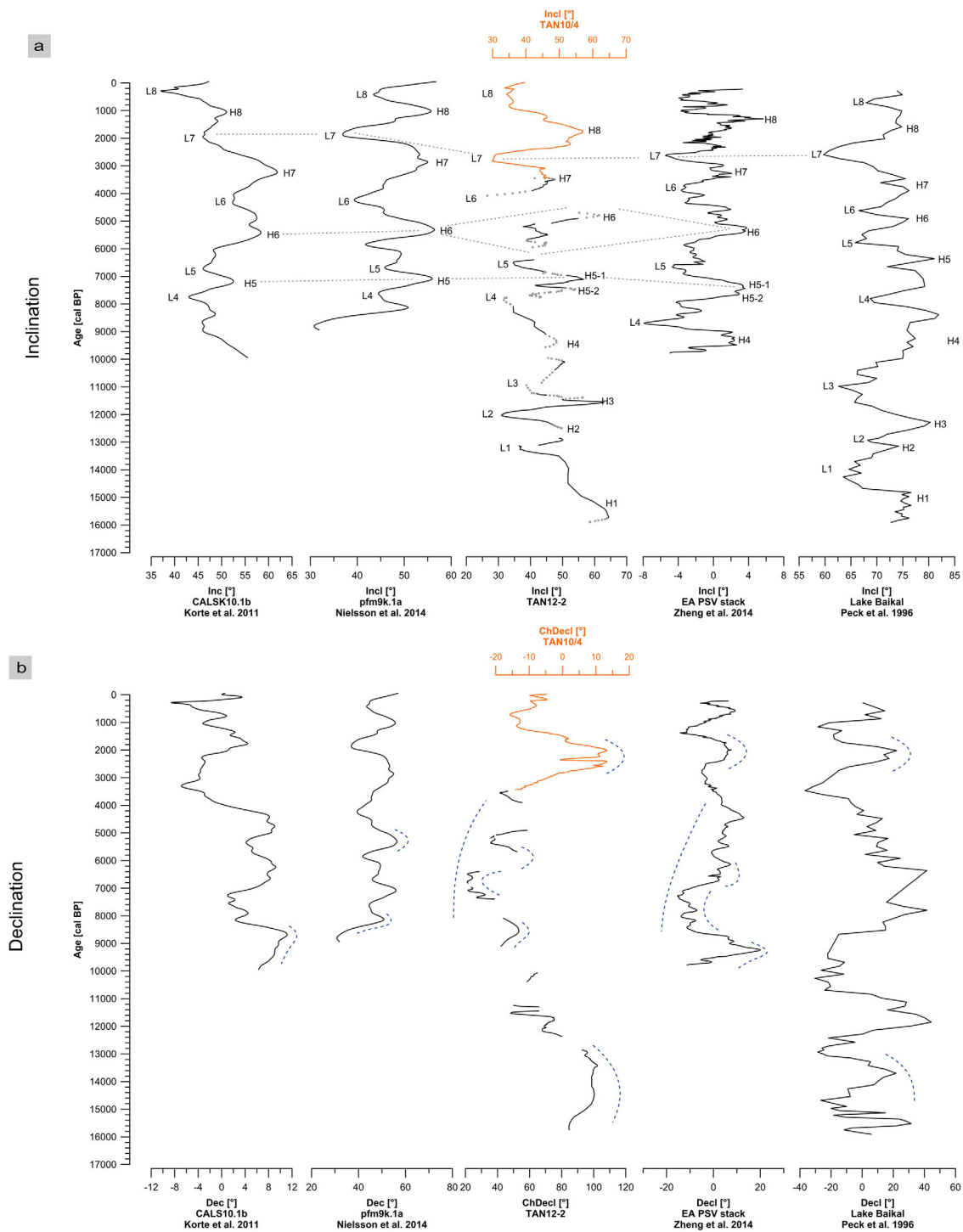


Figure 8. Comparison of the inclination and declination pattern of Tangra Yumco with the EA PSV stack [Zheng et al., 2014] and Lake Baikal [Peck et al., 1996] as well as with the predictions of the models CALSK10.1b [Korte et al., 2011] and pfm9k.1a [Nilsson et al., 2014b]. Data gaps in the Tangra Yumco record are due to missing and disturbed material. Data points influenced by the edge effect produced at the top and bottom of each section and around turbidites are shown without interpolation. The upper part of the composite profile consists of gravity core TAN10/4 shown in a different color. (a) Inclination patterns with matched inclination maxima (H1-H8) and minima (L1-L8). (b) Declination patterns of the three records. Similar structures are indicated by dashed lines. Please note that TAN10/4 is on a different scale.

two-peak inclination maximum H5 is detected only 330 years later in the EA stack than in Tangra Yumco (Figure 8a). For the past 4 kyr, the temporal correlation is very good, especially for H7 and L7, where the age offsets are <200 years.

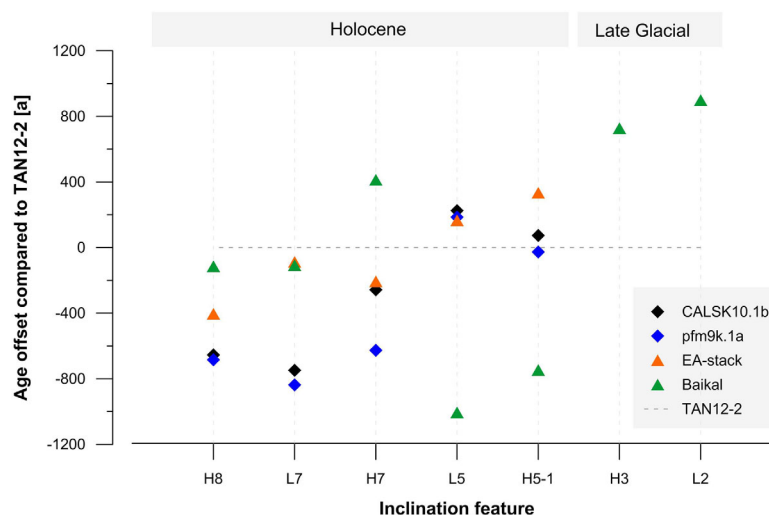


Figure 9. Age offsets of selected inclination features compared to Tangra Yumco (dashed line).

The mentioned age offsets between the records can have several reasons. The combined effects of lock-in depth and sedimentation rate, for example, produce a temporal lock-in delay. Besides the sedimentation rate, the lock-in depth depends on the thickness of the mixed zone (e.g., by bioturbation) [Roberts *et al.*, 2013]. Also in laminated sediments without bioturbation, a lock-in delay can be observed [Mellström *et al.*, 2015]. Additionally, uncertainties in the chronologies of the individual records have a major impact. For example, the analytical error for the radiocarbon ages from TAN12-2 is between 30 and 70 years, while during the calibration process, an age error between 100 and 540 years is calculated. Both mentioned causes for age-offsets (changing lock-in delay and uncertainties in the chronologies) in inclination and declination features commonly affect all sedimentary PSV archives [Mellström *et al.*, 2015; Nilsson *et al.*, 2014b].

7.4. Declination

When comparing the sedimentary records and model predictions, only a few comparable structures in the declination can be found between Tangra Yumco, both model predictions, the EA stack, and Lake Baikal, while the overall similarity between all records is quite low (Figure 8b). Not even both model predictions based on the same database document similar declination variations. Therefore, a direct comparison of the age offsets as done for the inclination is impossible. Although the corrections to obtain a relative declination record for Tangra Yumco might have affected its pattern, similar structures can be found in other records, especially for the past 4000 years.

An easterly declination swing between 16 and 13 ka cal B.P. is similar between Tangra Yumco and Lake Baikal. A further declination easterly swing around 9 ka cal B.P. is observed in Tangra Yumco, both model predictions, and the EA stack, but not in Lake Baikal. The overarching increasing declination trend between 8 and 4 ka cal B.P. in Tangra Yumco, that might be an artifact from relative declination corrections, is also found in the EA stack. For the past 4000 years, the declination pattern from Tangra Yumco compares almost perfectly to the EA stack and Lake Baikal, while both model predictions yield a very different pattern. Therefore, the application of declination as a stratigraphic tool for the Tibetan Plateau is still challenging and should be used with care and in combination with inclination variations only. Nonetheless, due to the similarity of the sedimentary declination records of the last 4000 years, more weight should be given to measured declinations than model predictions in this region.

7.5. Implications for Geomagnetic Field Variability and Stratigraphy

The inclination pattern of Tangra Yumco is broadly similar to both geomagnetic field model predictions, as well as to the EA stack and Lake Baikal. The age offsets of distinctive inclination features between all records are not consistent and differ in various time slices (Figure 9). Nevertheless, the good fit to the EA stack with only small age offsets of <400 years during the Holocene highlights the great potential of the newly obtained Tangra Yumco record for further paleomagnetic investigations in this region and the construction

of a PSV reference curve for central Asia. Although small-scale inclination changes recorded in the EA stack are smoothed by the u-channel measurements in Tangra Yumco, the three inclination peaks on top of H8 are visible in the EA stack and Tangra Yumco, hinting to a regional geomagnetic feature. In addition, the similar inclination patterns over such a large distance (Baikal and EA stack located 3000 km away from Tangra Yumco) suggest that large-scale core dynamics producing the PSV are plausible. For the Tibetan Plateau, this was already shown for the past 4000 years [Haberzettl *et al.*, 2015]. Further large-scale geomagnetic field changes over a distance of up to 5000 km were already observed spanning a region from western North America over eastern North America and Iceland to Fennoscandinavia [Barletta *et al.*, 2010b].

8. Conclusions

Paleomagnetic investigation on u-channels from Lake Tangra Yumco established the first PSV record for central Asia covering the past 15.9 ka cal B.P. A strong and stable single-component magnetization carried by low-coercivity minerals such as magnetite in the pseudo single domain state reveals a robust inclination record oscillating around the GAD for the past 15.9 ka cal B.P. Declination is less comparable than inclination, but shows a robust intralake and regional comparability for the past 4000 years. The inclination pattern on a regional scale reveal a good match to the EA stack and Lake Baikal, although they are located quite far away from one another implying large-scale geomagnetic field variations. Age offsets can be explained by uncertainties in the radiocarbon-based chronologies and variations in the lock-in delay. Geomagnetic field model predictions are in accordance with Tangra Yumco, assessing the quality of the models, although a large age offset is observed for the past 4000 years.

Although the new PSV record from Tangra Yumco is a step forward in establishing magnetostratigraphic research on the Tibetan Plateau, further research is required. A broader PSV database for the Tibetan Plateau and adjacent areas is needed to resolve remaining uncertainties in the timing of inclination and declination features. Further research would strengthen magnetostratigraphy as a possible dating tool on the Tibetan Plateau and help to refine global geomagnetic field models and therefore the knowledge of the Earth's magnetic field.

Acknowledgments

The data are available at <http://doi.pangaea.de/10.1594/PANGAEA.856970>. We gratefully acknowledge funding from the German Research Foundation (DFG) priority program 1372: "TiP: Tibetan Plateau – Formation – Climate – Ecosystems" (grant MA1308/23–2), the National Natural Science Foundation of China (grant 41271225), the Natural Sciences and Engineering Research Council of Canada (grant 312343-2012), and the Canadian Foundation for Innovation (grant 10738). For the support during field campaign, we thank our Sino-German team and especially Richard Niederreiter for his precious expertise during coring. For their support and help during the paleomagnetic measurements in Rimouski, we thank Julie Velle and Elissa Barris who conducted AGM measurements. This study also benefitted from two Young Scientist and Early Career Program Scholarships to Torsten Haberzettl awarded by the steering committee of the DFG priority program 1372. For providing their directional and intensity data from Lake Biwa and Lake Baikal for comparison, we thank Y. Zheng, A. Hayashida, and J. A. Peck. We also thank Jacques Labrie for providing a modified version of the GRADISTAT software. The seismic profile was provided by Thomas Kasper. Finally, Karoline Henkel wants to thank the Max Planck Society for her PhD scholarship.

References

- Ahlborn, M., *et al.* (2015), Sediment dynamics and hydrologic events affecting small lacustrine systems on the southern-central Tibetan Plateau—The example from the TT Lake, *Holocene*, 25, 508–522.
- Akita, L. G., P. Frenzel, T. Haberzettl, T. Kasper, J. Wang, and K. Reicherter (2015), Ostracoda (Crustacea) as indicators of subaqueous mass movements: An example from the large brackish lake Tangra Yumco on the southern Tibetan Plateau, China, *Palaeogeogr. Palaeoclimatol. Palaeoecol.*, 419, 60–74.
- Ali, M., H. Oda, A. Hayashida, K. Takemura, and M. Torii (1999), Holocene palaeomagnetic secular variation at Lake Biwa, central Japan, *Geophys. J. Int.*, 136, 218–228.
- Anson, G. L., and K. P. Kodama (1987), Compaction-induced inclination shallowing of the post-depositional remanent magnetization in a synthetic sediment, *Geophys. J. Int.*, 88, 673–692.
- Barletta, F., G. St-Onge, J. E. T. Channell, and A. Rochon (2010a), Dating of Holocene western Canadian Arctic sediments by matching paleomagnetic secular variation to a geomagnetic field model, *Quat. Sci. Rev.*, 29, 2315–2324.
- Barletta, F., G. St-Onge, J. S. Stoner, P. Lajeunesse, and J. Locat (2010b), A high-resolution Holocene paleomagnetic secular variation and relative paleointensity stack from eastern Canada, *Earth Planet. Sci. Lett.*, 298, 162–174.
- Blott, S. J., and K. Pye (2001), GRADISTAT: A grain size distribution and statistics package for the analysis of unconsolidated sediments, *Earth Surf. Processes Landforms*, 26, 1237–1248.
- Bloxham, J., and D. Gubbins (1985), The secular variation of Earth's magnetic field, *Nature*, 317, 777–781.
- Bressler, S. L., and D. P. Elston (1980), Declination and inclination errors in experimentally deposited specularite-bearing sand, *Earth Planet. Sci. Lett.*, 48, 227–232.
- Croudace, I. W., A. Rindby, and R. G. Rothwell (2006), ITRAX: Description and evaluation of a new multi-function X-ray core scanner, *Geol. Soc. Spec. Publ.*, 267, 51–63.
- Day, R., M. Fuller, and V. A. Schmidt (1977), Hysteresis properties of titanomagnetites: Grain-size and compositional dependence, *Phys. Earth Planet. Inter.*, 13, 260–267.
- Frank, U. (2007), Palaeomagnetic investigations on lake sediments from NE China: A new record of geomagnetic secular variations for the last 37 ka, *Geophys. J. Int.*, 169, 29–40.
- Gao, Y., Z. Hou, B. S. Kamber, R. Wei, X. Meng, and R. Zhao (2007), Lamproitic rocks from a continental collision zone: Evidence for recycling of subducted tethyan oceanic sediments in the mantle beneath southern Tibet, *J. Petrol.*, 48, 729–752.
- Gómez-Paccard, M., J. C. Larrasoña, S. Giral, and A. P. Roberts (2012), First paleomagnetic results of mid- to late Holocene sediments from Lake Issyk-Kul (Kyrgyzstan): Implications for paleosecular variation in central Asia, *Geochem. Geophys. Geosyst.*, 13, Q03019, doi:10.1029/2011GC004015.
- Haberzettl, T. (2015), Advances in limnogeology and paleolimnology with a special focus on corroborated chronologies using paleomagnetic secular variations, Habilitation thesis, 542 pp., Friedrich Schiller Univ., Jena, Germany.

- Haberzettl, T., G. St-Onge, H. Behling, and W. Kirleis (2013), Evaluating Late Holocene radiocarbon-based chronologies by matching palaeomagnetic secular variations to geomagnetic field models: An example from Lake Kalimpa (Sulawesi, Indonesia), *Geol. Soc. Spec. Publ.*, *373*, 245–259.
- Haberzettl, T., et al. (2015), Independently dated paleomagnetic secular variation records from the Tibetan Plateau, *Earth Planet. Sci. Lett.*, *416*, 98–108.
- Hyodo, M., A. Yoshihara, K. Kashiwaya, T. Okimura, T. Masuzawa, R. Nomura, S. Tanaka, T. B. Xing, L. S. Qing, and L. S. Jian (1999), A Late Holocene geomagnetic secular variation record from Erhai Lake, southwest China, *Geophys. J. Int.*, *136*, 784–790.
- Jackson, A., A. R. T. Jonkers, and M. R. Walker (2000), Four centuries of geomagnetic secular variation from historical records, *Philos. Trans. R. Soc. London A*, *358*, 957–990.
- Kasper, T., T. Haberzettl, S. Doberschütz, G. Daut, J. Wang, L. Zhu, N. Nowaczyk, and R. Mäusbacher (2012), Indian Ocean Summer Monsoon (IOSM)-dynamics within the past 4 ka recorded in the sediments of Lake Nam Co, central Tibetan Plateau (China), *Quat. Sci. Rev.*, *39*, 73–85.
- Kirschvink, J. L. (1980), The least-squares line and plane and the analysis of palaeomagnetic data, *Geophys. J. Int.*, *62*, 699–718.
- Korhonen, K., F. Donadini, P. Riisager, and L. J. Pesonen (2008), GEOMAGIA50: An archeointensity database with PHP and MySQL, *Geochem. Geophys. Geosyst.*, *9*, Q04029, doi:10.1029/2007GC001893.
- Korte, M., and C. G. Constable (2005), The geomagnetic dipole moment over the last 7000 years—New results from a global model, *Earth Planet. Sci. Lett.*, *236*, 348–358.
- Korte, M., F. Donadini, and C. G. Constable (2009), Geomagnetic field for 0–3 ka: 2. A new series of time-varying global models, *Geochem. Geophys. Geosyst.*, *10*, Q06008, doi:10.1029/2008GC002297.
- Korte, M., C. G. Constable, F. Donadini, and R. Holme (2011), Reconstructing the Holocene geomagnetic field, *Earth Planet. Sci. Lett.*, *312*, 497–505.
- Long, H., T. Haberzettl, S. Tsukamoto, J. Shen, T. Kasper, G. Daut, L. Zhu, R. Mäusbacher, and M. Frechen (2015), Luminescence dating of lacustrine sediments from Tangra Yumco (southern Tibetan Plateau) using post-IR IRSL signals from polymineral grains, *Boreas*, *44*, 139–152.
- Mazaud, A. (2005), User-friendly software for vector analysis of the magnetization of long sediment cores, *Geochem. Geophys. Geosyst.*, *6*, Q12006, doi:10.1029/2005GC001036.
- Mellström, A., A. Nilsson, T. Stanton, R. Muscheler, I. Snowball, and N. Suttie (2015), Post-depositional remanent magnetization lock-in depth in precisely dated varved sediments assessed by archaeomagnetic field models, *Earth Planet. Sci. Lett.*, *410*, 186–196.
- Miehe, S., G. Miehe, J. F. N. Leeuwen, C. Wrozyna, W. O. Knaap, L. Duo, and T. Haberzettl (2014), Persistence of Artemisia steppe in the Tangra Yumco Basin, west-central Tibet, China: Despite or in consequence of Holocene lake-level changes?, *J. Paleolimnol.*, *51*, 267–285.
- Nakagawa, T. (2007), Double-L channel: An amazingly non-destructive method of continuous sub-sampling from sediment cores, paper presented at XVII INQUA Congress, Cairns, Queensland, Australia, Department of Geography, University of Newcastle-upon-Tyne, U. K.
- Nilsson, A., R. Holme, M. Korte, N. Suttie, and M. Hill (2014b), Reconstructing Holocene geomagnetic field variation: New methods, models and implications, *Geophys. J. Int.*, *198*, 229–248.
- Ólafsdóttir, S., Á. Geirsdóttir, G. H. Miller, J. S. Stoner, and J. E. T. Channell (2013), Synchronizing Holocene lacustrine and marine sediment records using paleomagnetic secular variation, *Geology*, *41*, 535–538.
- Peck, J., J. King, S. Colman, and V. Kravchinsky (1996), An 84-kyr paleomagnetic record from the sediments of Lake Baikal, Siberia, *J. Geophys. Res.*, *101*, 11,365–11,385.
- Rades, E. F., R. Hetzel, Q. Xu, and L. Ding (2013), Constraining Holocene lake-level highstands on the Tibetan Plateau by ^{10}Be exposure dating: A case study at Tangra Yumco, southern Tibet, *Quat. Sci. Rev.*, *82*, 68–77.
- Reimer, P. J., et al. (2013), IntCal13 and marine13 radiocarbon age calibration curves 0–50,000 years cal BP, *Radiocarbon*, *55*, 1869–1887.
- Roberts, A. P., L. Tauxe, and D. Heslop (2013), Magnetic paleointensity stratigraphy and high-resolution Quaternary geochronology: Successes and future challenges, *Quat. Sci. Rev.*, *61*, 1–16.
- Snowball, I., and P. Sandgren (2002), Geomagnetic field variations in northern Sweden during the Holocene quantified from varved lake sediments and their implications for cosmogenic nuclide production rates, *Holocene*, *12*, 517–530.
- Stoner, J. S., and G. St-Onge (2007), Chapter Three Magnetic stratigraphy in paleoceanography: Reversals, excursions, paleointensity, and secular variation, in *Developments in Marine Geology*, edited by C. Hillaire-Marcel and A. De Vernal, vol. 1, chap. 3, pp. 99–138, Elsevier, Amsterdam, Netherlands.
- St-Onge, G., and J. S. Stoner (2011), Paleomagnetism near the North Magnetic Pole: A unique vantage point for understanding the dynamics of the geomagnetic field and its secular variations, *Oceanography*, *24*, 42–50.
- St-Onge, G., T. Mulder, D. J. W. Piper, C. Hillaire-Marcel, and J. S. Stoner (2004), Earthquake and flood-induced turbidites in the Saguenay Fjord (Québec): A Holocene paleoseismicity record, *Quat. Sci. Rev.*, *23*, 283–294.
- Stuiver, M., and P. J. Reimer (1993), Extended (super 14) C data base and revised CALIB 3.0 (super 14) C age calibration program, *Radiocarbon*, *35*, 215–230.
- Su, Y., X. Gao, Q. Liu, J. Wang, T. Haberzettl, L. Zhu, J. Li, Z. Duan, and L. Tian (2013a), Mineral magnetic study of lacustrine sediments from Lake Pumoyum Co, southern Tibet, over the last 19 ka and paleoenvironmental significance, *Tectonophysics*, *588*, 209–221.
- Su, Y., et al. (2013b), Mechanism of variations in environmental magnetic proxies of lake sediments from Nam Co, Tibet during the Holocene, *Chin. Sci. Bull.*, *58*, 1568–1578.
- Tauxe, L. (1993), Sedimentary records of relative paleointensity of the geomagnetic field: Theory and practice, *Rev. Geophys.*, *31*, 319–354.
- Tauxe, L., K. P. Kodama, and D. V. Kent (2008), Testing corrections for paleomagnetic inclination error in sedimentary rocks: A comparative approach, *Phys. Earth Planet. Inter.*, *169*, 152–165.
- Wang, J., L. Zhu, Y. Wang, P. Peng, Q. Ma, T. Haberzettl, T. Kasper, T. Matsunaka, and T. Nakamura (2015), Variability of the ^{14}C reservoir effect in lake Tangra Yumco, Central Tibet (China), determined from recent sedimentation rates and dating of plant fossils, *Quat. Int.*, doi:10.1016/j.quaint.2015.10.084, in press.
- Weeks, R., C. Laj, L. Endignoux, M. Fuller, A. Roberts, R. Manganne, E. Blanchard, and W. Goree (1993), Improvements in long-core measurement techniques: Applications in palaeomagnetism and palaeoceanography, *Geophys. J. Int.*, *114*, 651–662.
- Yang, X., F. Heller, J. Yang, and Z. Su (2009), Paleosecular variations since ~9000 yr BP as recorded by sediments from maar lake Shuangchiling, Hainan, South China, *Earth Planet. Sci. Lett.*, *288*, 1–9.
- Yang, X., Q. Liu, Z. Duan, Z. Su, G. Wei, G. Jia, T. Ouyang, Y. Su, and L. Xie (2012), A Holocene palaeomagnetic secular variation record from Huguangyan maar Lake, southern China, *Geophys. J. Int.*, *190*, 188–200.

- Zheng, Y., H. Zheng, C. Deng, and Q. Liu (2014), Holocene paleomagnetic secular variation from East China Sea and a PSV stack of East Asia, *Phys. Earth Planet. Inter.*, *236*, 69–78.
- Zhu, L., P. Zhang, W. Xia, B. Li, and L. Chen (2003), 1400-year cold/warm fluctuations reflected by environmental magnetism of a lake sediment core from the Chen Co, southern Tibet, China, *J. Paleolimnol.*, *29*, 391–401.
- Zijderveld, J. D. A. (1967), AC demagnetization of rocks: Analysis of results, in *Methods in Paleomagnetism*, edited by D. W. Collinson, K. M. Creer, and S. K. Runcorn, pp. 254–286, Elsevier, Amsterdam.